Acta Myologica • 2018; XXXVII: p. 193-203

ORIGINAL ARTICLES

Kir2.2 p.Thr140Met: a genetic susceptibility to sporadic periodic paralysis

Chunxiang Fan[1*], Marius Kuhn[2*], Alexander Pepler MBiol[3], James Groome[4], Vern Winston[4], Saskia Biskup[3], Frank Lehmann-Horn[1**] and Karin Jurkat-Rott[1]

[1] Division of Neurophysiology, Ulm University, Germany; [2] Genetikum, Neu-Ulm, Germany; [3] CeGaT GmbH, Tübingen, Germany; [4] Department of Biological Sciences, Idaho State University, Pocatello, USA

Introduction. Periodic paralyses (PP) are recurrent episodes of flaccid limb muscle weakness. Next to autosomal dominant forms, sporadic PP (SPP) cases are known but their genetics are unclear.

Methods. In a patient with hypokalemic SPP, we performed exome sequencing to identify a candidate gene. We sequenced this gene in 263 unrelated PP patients without any known causative mutations. Then we performed functional analysis of all variants found and molecular modelling for interpretation.

Results. Exome sequencing in the proband yielded three heterozygous variants predicted to be linked to disease. These encoded p.Thr140Met in the Kir2.2 potassium channel, p.Asp229Asn in protein kinase C theta, and p.Thr15943Ile in titin. Since all hitherto known causative PP genes code for ion channels, we studied the Kir2.2-encoding gene, *KCNJ12*, for involvement in PP pathogenesis. *KCNJ12* screening in 263 PP patients revealed three further variants, each in a single individual and coding for p.Gly419Ser, p.Cys75Tyr, and p.Ile283Val. All four Kir2.2 variants were functionally expressed. Only p.Thr140Met displayed relevant functional alterations, i.e. homo-tetrameric channels produced almost no current, and hetero-tetrameric channels suppressed co-expressed wildtype Kir2.1 in a dominant-negative manner. Molecular modelling showed Kir2.2 p.Thr140Met to reduce movement of potassium ions towards binding sites in the hetero-tetramer pore compatible with a reduced maximal current. MD simulations revealed loss of hydrogen bonding with the p.Thr140Met substitution.

Discussion. The electrophysiological findings of p.Thr140Met are similar to those found in thyrotoxic PP caused by Kir2.6 mutations. Also, the homologous Thr140 residue is mutated in Kir2.6. This supports the idea that Kir2.2 p.Thr140Met conveys susceptibility to SPP and should be included in genetic screening.

Key words: periodic paralysis, susceptibility gene, Kir2.2 channel, Kir2.1 channel, hetero-tetramer

Introduction

The periodic paralyses (PPs) are characterised by recurrent bouts of flaccid limb muscle weakness often accompanied by alteration in serum potassium level (1). PP can be divided into familial PP (FPP), thyrotoxic PP (TPP), and sporadic PP (SPP) based on relative genotype-phenotype correlations. Fully penetrant dominant mutations are observed in FPP, incomplete penetrance exacerbated by thyrotoxicosis is characteristic of TPP, and incomplete penetrance with an unknown exacerbation factor or multifactorial causes underlies SPP.

With respect to pathogenesis, PPs result from sustained muscular depolarization that abolishes action potentials (APs). Causative mutations are located in the *SCN4A* gene encoding the sodium channel Nav1.4 initiating the AP, the *CACNA1S* gene encoding the calcium channel Cav1.1 coupling the AP to contraction, or the *KCNJ2* and *KCNJ18* genes encoding the potassium channels Kir2.1 and Kir2.6 that maintain the resting potential (2). Underlying mechanisms of these mutations include i) disruption of channel inactivation of Nav1.4 resulting in persistent currents, ii) leaky S4 voltage senor domains of Nav1.4 and Cav1.1 resulting in short-circuit inward cation currents, and iii) reduced conductance of the inwardly rectifying Kir potassium currents (2-5). The goal of our study was to look for a putative additional genetic cause in a single individual with hypokalemic SPP, an SPP form with ictal drop of serum potassium.

* Equal contribution to first author

**Dedicated to the late Prof. Dr. Frank Lehmann-Horn who faithfully contributed to this work until his death on May 8th, 2018. We hereby thank him for his constant support and his continued optimism in the research field of ion channelopathies.

Address for correspondence: Marius Kuhn, Genetikum, Wegenerstraße 15, 89231 Neu-Ulm, Germany. E-mail: Kuhn@genetikum.de

Patients and methods

Patients

Informed consent was obtained from the proband with hypokalemic PP, and was already given for an additional 263 PP patients who were referred earlier for genetic consultation. Of the latter, 29 had FPP, 25 had TPP, and 209 had SPP. Clinical diagnosis was based on patient history provided by the referring physician. PP was diagnosed if the patient had at least two episodes of flaccid quadriplegia. FPP was diagnosed if, additionally, a parent, a sibling, or an offspring of the patient were clinically affected. TPP was diagnosed if there was concomitant hyperthyroidism present, and SPP was diagnosed for isolated cases. All patients had been tested negative for known pathogenic variants in *SCN4A*, *CACNA1S*, *KCNJ2*, and *KCNJ18* genes. All procedures were approved by the Ethics Committee of Ulm University.

Exome sequencing

To determine the genetic cause of hypokalemic SPP in the proband, DNA was enriched with the SureSelectXT V5 exome kit (Agilent Technologies) and sequenced on a HiSeq 2500 Illumina sequencer. About 195 million paired reads of 100 bp length were produced. Reads were de-multiplexed with Casava version 1.8.2 (Illumina) and adapter sequences removed with Skewer version 0.1.116. Trimmed reads were mapped with Burrows-Wheeler Aligner version 0.7.2 (6) against the human reference genome hg19 (UCSC), yielding an average coverage of 155. Variant calling was performed using VarScan version 2.3.5 and Samtools version 0.1.18 (7). Calls were annotated using the Database of Single-Nucleotide Polymorphisms (dbSNP, www.ncbi.nlm.nih.gov/snp).

Variants potentially changing the protein were analysed further, i.e. non-synonymous SNPs, changes of initiation or stop codons, splicing variants, and in-frame or frameshifting insertions or deletions. Filtering was performed by excluding all variants more frequent than 0.5% as listed in dbSNP or UCSC Table Browser (www.genome.ucsc.edu) and requiring expression in skeletal muscle according to the Human Protein Atlas (320 genes, www.proteinatlas.org). The resulting variants were preliminarily interpreted using the protein prediction tools Polyphen-2 (www.genetics.bwh.harvard.edu/pph2), MutationTaster (www.mutationtaster.org), and Sift (www.sift.jcvi.org).

Sanger sequencing

To confirm the presence of the identified *KCNJ12* variant in the proband sample, the coding region of *KCNJ12* was sequenced. Subsequently, *KCNJ12* was sequenced in the remaining 263 DNA samples to check for recurrence in PP. The coding region of *KCNJ12* was amplified using a gene-specific nested polymerase chain reaction (PCR) with two specific primers (forward: CCAGACATGCTGTCGTCTCTGTTG; reverse: GGGCCTCTCCCCAGCCG). The resulting products were sequenced using the forward-primers (CCAGACATGCTGTCGTCTCTGTTG/CTGGCGGTACATGCTGCTCATC/CGCCGTGGTGGCCCTGCGTGAC/GCCAATGAGATCCTGTGGGGTCAC). Potential pathogenicity of the variants was preliminarily interpreted using the prediction tools Polyphen-2, Mutation Taster, and Sift. Additionally, to exclude mapping problems of the exome sequencing in the proband sample, the coding region of the known PP gene *KCNJ18* was sequenced in the proband sample using the gene-specific nested PCR technique previously described (8).

Electrophysiological study

For functional expression of the identified variants, the human *KCNJ12* subunit was sub-cloned into the pcDNA3.1 vector and site-directed mutagenesis of base changes coding for p.Thr140Met, p.Gly419Ser, p.Cys75Tyr, and p.Ile283Val variants was performed by an external lab (GATC Biotech). The human *KCNJ2* subunit was cloned into the pcDNA3.1 vector by the same external lab. Whole-cell patch clamp recordings were performed after transient transfection of human tsA201 cells with *KCNJ12* (0.2 µg) and pEGFP (0.05 µg) or, in co-expression studies, *KCNJ12* (0.1 µg) with *KCNJ2* (0.1 µg) and pEGFP (0.05 µg). Transfected cells were identified by GFP fluorescence. Potassium currents were recorded without leak subtraction after partial series resistance compensation (~ 85%) using an Axopatch 200B amplifier (Molecular Devices). The pipette resistance was approximately 1.5 MΩ after filling with internal solution containing (in mM): Potassium gluconate 110, KCl 20, HEPES 10, EGTA 10, $MgCl_2.^6H_2O$ 1, Na_2ATP 5, glucose 5. The external solution contained (in mM): NaCl 117, KCl 30, $CaCl_2.2H_2O$ 2, $MgCl_2.^6H_2O$ 1, glucose 5, $NaHCO_3$ 2, HEPES 10. In some experiments, external KCl was reduced to 5mM and NaCl increased to 142 mM. The pH was adjusted to 7.3 and 7.4 for external and internal solutions, respectively, and osmolarity was ~300 mOsm. Data are presented as mean ± standard error of the mean (SEM). Student's t-tests were applied for statistical evaluation with significance levels set to $p < 0.05$.

Fluorescence imaging

To compare trafficking of wildtype channels to the p.Thr140Met variant, coding Kir2.2 regions were

sub-cloned into pEGFP vectors whereby EGFP was fused to the N-terminus of the region by an external lab (GATC Biotech). Transfected tsA cells cultured on 11 mm glass cover slips were fixed with paraffin, images were taken with fixed exposure time on an Axioskop 2 microscope with AxioCamMR3 and EC Plan-Neofluar 40x/1.30 oil lens (Zeiss), and the GFP detection was filtered as for Alexa 488. Membrane areas over the cytoplasm of the cells and background were analyzed as mean gray values with ImageJ. For quantification, background values were subtracted from the membrane values for each cell.

Molecular modelling

The crystal structure of a prokaryotic inwardly rectifying Kir channel (KirBac 3.1) was used as template for homology modelling of mammalian *KCNJ12* and *KCNJ2* (9). Clustal amino acid alignment of mammalian Kir channels encoded by *KCNJ1-15*, the Gallus gallus Kir2.2 channel, and KirBac3.1 channels was used in the production of homology models of human wildtype (WT) Kir2.1, WT Kir2.2, and variant p.Thr140Met Kir2.2. For these models, we used the structure file 4lp8.pdb (KirBac3.1)9 as template in MODELLER. Potassium ion coordinates were saved for the A chain in the Kir2.2 model, and tetramers of Kir2.2-Kir2.1 were constructed. Tetrameric models were then equilibrated to relieve subunit clashes and allowed to reach an energy minimum, with Chimera (10). The energy minimized tetramers were used to visualize the distribution of potassium ions with respect to the selectivity filter.

The quantitative impact of the p.Thr140Met variant was assessed with molecular dynamics (MD) simulations. Equilibrated models of KirWT2.2-KirWT2.1 or KirT140M2.2-KirWT2.1 (equimolar ratio of Kir2.2 and Kir2.1) were incorporated into POPC (1-palmitoyl 2-oleoyl-sn-glycero-3-phosphocholine) lipid bilayers, solvated with TIPW water molecules and 0.2M KCl, and equilibrated for lipid and protein minimization, using VMD (visual molecular dynamics). Simulations were run in NAMD (not another molecular dynamics) with application of a CHARMM force field with Langevin dynamics at -600 mV. Trajectories of distance between the carboxyl of Glu139 and Thr140 (WT) or Met140 (variant) were calculated using the PLUMED plug-in, and trajectories of hydrogen bonding between Glu139 and Ile144 of the selectivity filter motif (TIGYG) were calculated using the H-bonding plug-in of VMD. Hydrogen bonding between analogous pairs is a critical step in early permeation of K+ ions through the selectivity filter in KcsA (11).

Results

Proband phenotype

The phenotype description of the proband is based on the medical file excerpts sent by the referring physician with the patient's consent. The proband did not volunteer further information and denied additional examination and biopsy. He experienced only two documented episodes of quadriplegic weakness in his life, at age 18 and 30 years, both lasting 12 hours. During the second, serum potassium level was 1.88 mmol/L and potassium administration relieved the symptoms. Thyroid hormones levels were normal. The patient reported no cardiac arrhythmia and no dysmorphic features as would be typical for Andersen-Tawil syndrome. No relatives were known to be affected by PP. We classified the phenotype as very mild, hypokalemic SPP.

Exome sequencing

Altogether, 83,246 variants were detected in the sample of the proband, including redundant listings of the same variant in different splice isoforms. Elimination of intronic and synonymous changes reduced the number of variants including redundancies down to 17,880. Filtering by allele frequencies for variants more rare than 0.5% reduced the number of variants to 2,685. Filtering for muscle-specific expression (i.e. the 320 muscle specific genes according the Human Protein Atlas) and eliminating the redundant listings left 31 variants. These were preliminarily interpreted using Polyphen2, MutationTaster, and Sift (Table 1). Since these programs cannot interpret consequences of splicing variants, the two identified splice variants could not be analysed further. Of the remaining variants, only three were predicted to be linked to disease by at least two of the prediction programs: a *KCNJ12* variant c.419C > T coding for p.Thr140Met in the Kir2.2 channel, a *PRKCQ* variant c.685G > A coding for p.Asp229Asn in protein kinase C theta, and a *TTN* variant c.47828C > T coding for p.Thr15943Ile in titin. All three of these variants were present in a heterozygous state. None of the three variants have been, to our knowledge, reported to be associated to disease in the literature. Since all hitherto known causative PP genes encode ion channels, we opted to further study only the *KCJN12* variant.

Sanger sequencing

The presence of the heterozygous c.419C > T base change in *KCNJ12* coding for p.Thr140Met in Kir2.2 was confirmed using Sanger sequencing (Fig. 1, top). Since a homologous p.Thr140Met in Kir2.6 encoded by *KCNJ18* was reported previously (12), we confirmed absence of

Table 1. Exome sequencing proband.

Gene	Base change	Protein change	SNP	Allele frequency	Poly-phen2	Mutation taster	Sift
ACTN3	c.2385C > G	p.Asp795Glu	n.a.	n.a.	Benign	Pseudogene	n.a.
AGBL1	c.774_779dupAGATGA	p.Glu258_ Asp259dup	rs775629809	0.000017	n.a.	Polymorphism	n.a.
CLIC5	c.237A > T	p.Arg79Ser	rs41271277	0.002805	Benign	Polymorphism	Tolerated
FHL3	c.331 + 7G > C	splice variant	rs4570384	0.000594	n.a.	n.a.	n.a.
HRC	c.1001G > A	p.Gly334Asp	rs796956072	n.a.	Benign	Polymorphism	Tolerated
HRC	c.992C > A	p.Ala331Asp	rs763482766	0.000017	Benign	Polymorphism	Tolerated
HRC	c.986T > A	p.Val329Asp	rs138152757	0.000042	Benign	Polymorphism	Tolerated
HRC	c.744T > A	p.Asp248Glu	n.a.	n.a.	Benign	Polymorphism	Tolerated
HRC	c.738T > A	p.Asp246Glu	n.a.	n.a.	Benign	Polymorphism	Tolerated
HRC	c.730G > A	p.Glu244Lys	rs775263588	0.000817	Benign	Polymorphism	Tolerated
HRC	c.722A > G	p.Gln241Arg	rs773435857	0.000784	Benign	Polymorphism	Tolerated
HRC	c.703G > A	p.Gly235Ser	rs760105084	0.000746	Benign	Polymorphism	Tolerated
HRC	c.689G > A	p.Gly230Glu	rs756913154	0.000690	Benign	Polymorphism	Tolerated
IGFN1	c.4646C > G	p.Thr1549Arg	rs199718718	n.a.	n.a.	Polymorphism	Tolerated
IGFN1	c.4715C > T	p.Ala1572Val	rs201241861	0.000090	n.a.	Polymorphism	Tolerated
IGFN1	c.4728G > A	p.Met1576Ile	n.a.	n.a.	n.a.	Polymorphism	Tolerated
IGFN1	c.4747A > G	p.Ser1583Gly	rs199574248	n.a.	n.a.	Polymorphism	Tolerated
IGFN1	c.4823T > C	p.Val1608Ala	rs201505263	n.a.	n.a.	Polymorphism	Tolerated
IGFN1	c.4828G > A	p.Glu1610Lys	rs71524455	0.000962	n.a.	Polymorphism	Tolerated
IGFN1	c.4855G > A	p.Gly1619Ser	rs189258058	n.a.	n.a.	Polymorphism	Tolerated
IGFN1	c.5160G > A	p.Met1720Ile	rs200673977	0.000787	n.a.	Polymorphism	Tolerated
IGFN1	c.6016G > A	p.Glu2006Lys	rs12729404	0.000116	Benign	Polymorphism	Tolerated
IGFN1	c.6024A > G	p.Ile2008Met	rs12728986	0.000114	Benign	Polymorphism	Tolerated
IGFN1	c.6043G > A	p.Gly2015Ser	rs796090138	n.a.	Benign	Polymorphism	Tolerated
KCNJ12	c.419C > T	p.Thr140Met	rs536297311	0.000056	Probably damaging	Disease causing	Damaging
LRRC14B	c.310C > T	p.Arg104Cys	n.a.	n.a.	Benign	Polymorphism	Tolerated
MAFA	c.621_623delCCA	p.His208del	rs141816879	n.a.	n.a.	Polymorphism	n.a.
PPP1R3A	c.1428T > A	p.Asn476Lys	rs2974944	0.001129	Benign	Polymorphism	Tolerated
PRKCQ	c.685G > A	p.Asp229Asn	rs34524148	0.001052	Probably damaging	Disease causing	Tolerated
TTN	c.47828C > T	p.Thr1594Ile	rs776113556	0.000008	Probably damaging	Disease causing	n.a.
TTN	c.10361-5delT	Splice variant	rs58651353	n.a.	n.a.	n.a.	n.a.

n.a. = not available.

the corresponding homologous c.419C > T base change in the *KCNJ18* gene by Sanger Sequencing to exclude mapping problems of the exome analysis (Fig. 1, bottom). To test the possibility of the *KCNJ12* gene being generally linked to PP, we sequenced 263 PP samples in *KCNJ12* using the Sanger technique. No changes were detected in 249 samples; eleven samples had synonymous SNP (coding for 1x p.Arg214Arg, 8x p.Asp61Asp 1x p.Ser266Ser, 1x p.Asp291Asp), and three samples each had a different non-synonymous base change. The latter were: c.1255G > A coding for p.Gly419Ser (rs77266866) with an allele frequency of 0.00077 (consistently predicted to be benign), the not yet described c.224G > A coding for p.Cys75Tyr (consistently predicted to be pathogenic), and c.847A > G coding for p.Ile283Val (1x predicted to be pathogenic, 2x predicted to be benign) (Table 2).

The phenotypes for the three SPP cases with non-synonymous variants were briefly: i) for the p.Cys75Tyr carrier: onset at age 18, yearly quadriplegic episodes, ictal potassium of 1.5mM, episodes triggered by diarrhoea, fever, and sports, ii) for the p.Ile283Val carrier: onset at age 52, small fibre neuropathy, muscle jerking, cramps, myalgia, intermittent hypokalaemia with morning weakness lasting minutes, and iii) for the p.Gly419Ser carrier: two episodes in lifetime at age 22 and 28 lasting three hours, having concomitant myalgia, and being triggered by cortisol administration.

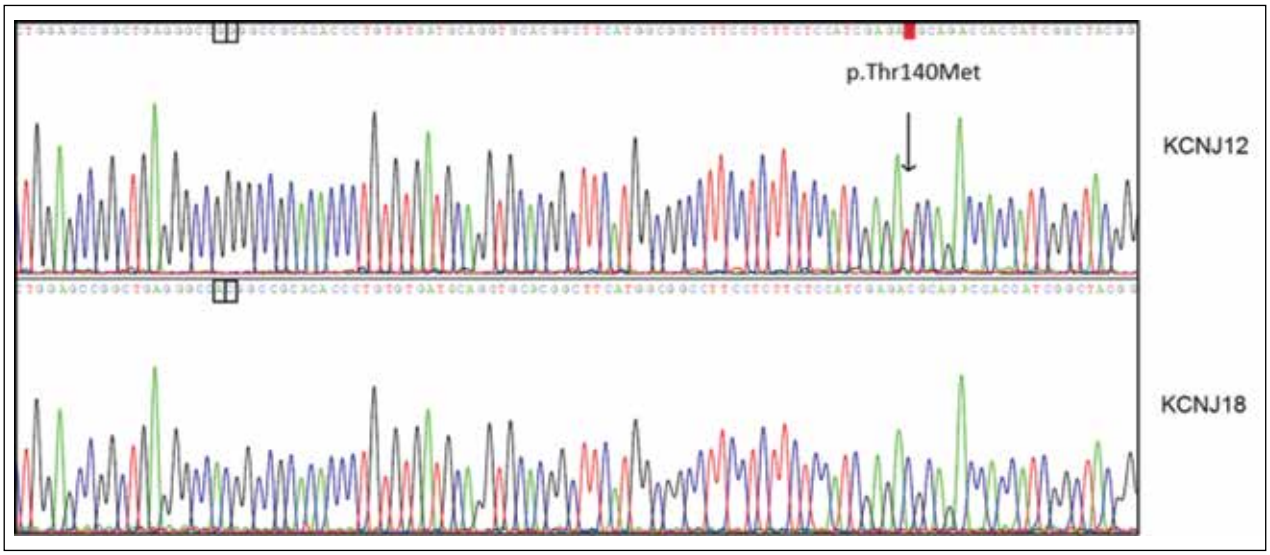

Figure 1. *Sanger sequencing proband.* Electropherogram of both genes, *KCNJ12* (top) and *KCNJ18* (bottom). The presence of a heterozygous c.419C > T base change coding for p.Thr140Met in the coding region of *KCNJ12* was confirmed using Sanger sequencing (red box). In *KCNJ18*, no base change was identified at this position. Additionally, two positions were marked (black boxes) to highlight the differences in wildtype sequences of these two genes in this highly homologous region proving the specificity of our amplification.

Table 2. Sanger sequencing *KCNJ12* in PP.

Base change	Protein change	SNP	Allele frequency	Poly-Phen2	Mutatio taster	Sift
c.224G > A	p.Cys75Tyr	n.a.	n.a.	Probably damaging	Disease causing	Damaging
c.847A > G	p.Ile283Val	n.a.	n.a.	Benign	Disease causing	Tolerated
c.1255G > A	p.Gly419Ser	rs77266866	0.00077	Benign	Polymorphism	Tolerated

n.a. = not available

The prediction results (Tables 1, 2) suggest i) that p.Gly419Ser would not be expected to cause any effects, ii) that the expectation for p.Ile283Val is unclear, and iii) that p.Cys75Tyr and p.Thr140Met would be expected to produce relevant changes in channel function. To test whether the prediction programs correctly assessed the disease-causing potency of the variants and, more specifically, to test whether p.Thr140Met may contribute to the SPP phenotype in the proband, we performed whole cell patch clamp studies on the four non-synonymous Kir2.2 variants.

Electrophysiology and fluorescence imaging

Kir currents were elicited from a holding potential of 0 mV in 10 mV-voltage steps of 100ms duration from hyperpolarized potentials – 80 mV to + 40 mV. In 30 mM external KCl, typical rectifier Kir currents were recorded from expression of Kir2.2-WT and the three variants p.Cys75Tyr, p.Ile283Val, and p.Gly419Ser. In contrast, no endogenous Kir currents were detected in untransfected cells or in cells expressing p.Thr140Met. However, when WT was co-expressed with p.Thr140Met, typical Kir currents could be observed (Fig. 2A).

These findings could indicate, among other possibilities, that p.Thr140Met channels are not synthesized, not inserted into the membrane, or not functional. To assess the subcellular localization of the p.Thr140Met channels in comparison with Kir2.2-WT, we performed fluorescence imaging. Both channel types were expressed uniformly on the plasma membrane, with gray levels of WT *vs* p.Thr140Met being 16.17 ± 0.95 *vs* 13.49 ± 1.11 (p = 0.08, n = 18-19) (Fig. 2B). This finding indicates that p.Thr140Met channels are observed at levels similar to WT in the plasma membrane 24 hours post-transfection which means that protein synthesis, trafficking, and membrane insertion are intact. Therefore, the effect of p.Thr140Met is more likely to be

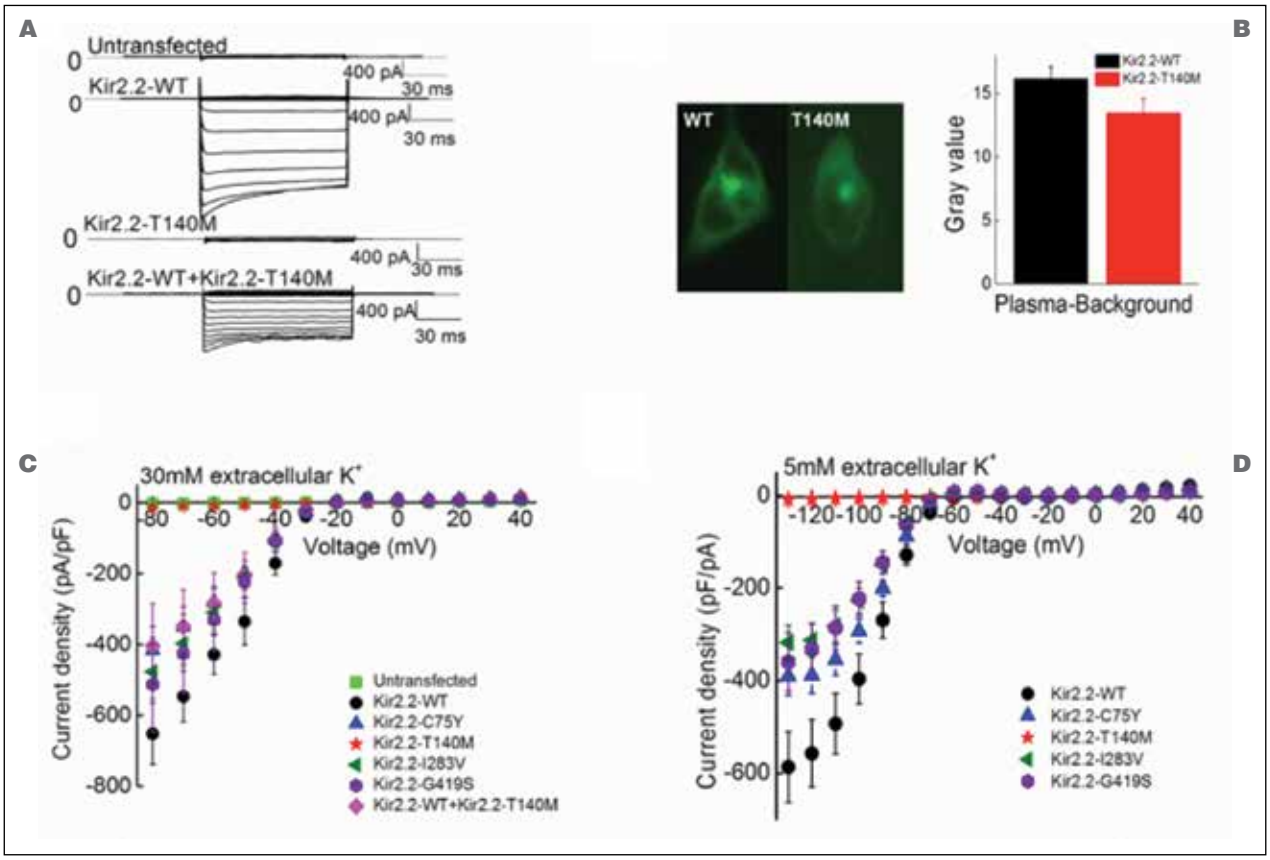

Figure 2. *Functional expression.* Functional characterization of Kir2.2-WT and four missense variants expressed in tsA 201 cells. **A)** Representative current traces. Note that p.Thr140Met channels do not produce a current. **B)** Fluorescence image of the tsa 201 cell expressing WT and p.Thr140Met Kir2.2 fusion proteins with GFP (Left). Mean grey values from the membrane areas after subtraction of background showed comparable signal intensity between WT (n = 18) and p.Thr140Met (n = 19) (Right). **C)** Normalized current-voltage relationships for untransfected cells (n = 9), WT (n = 19), p.Cys75Tyr (n = 15), p.Thr140Met (n = 16), p.Ile283Val (n = 15), p.Gly419Ser (n = 8) and Kir2.2-WT+Kir2.2-p.Thr140Met (n = 10) recorded in 30mM external K+. **D)** Normalized current-voltage relationships for WT (n = 10), p.Cys75Tyr (n = 11), p.Thr140Met (n = 15), p.Ile283Val (N = 11) and p.Gly419Ser (n = 11) recorded in 5mM external K+. Data are shown as means ± SEM.

due to a direct effect on channel function, a possibility that we focused further on using electrophysiology.

Plotting of the obtained current peaks against the voltage revealed almost linear current-voltage relationships (Fig. 2C). Conductances were calculated from the steepness of the current-voltage relationship in the voltage range from – 70 mV to – 40 mV. Conductances for the inward currents were 288.28±49.11 nS/pF for WT (n = 19), 308.49 ± 77.84 nS/pF for p.Gly419Ser (n = 8, p = 0.82), 275.36 ± 44.47 nS/pF for p.Ile283Val (n = 15, p = 0.85), 220.76 ± 37.39 nS/pF for p.Cys75Tyr (n = 15, p = 0.3), 2.67 ± 0.79 nS/pF for p.Thr140Met (n = 16, p < 0.001), and 216.47 + 64.36 for Kir2.2-WT-Kir2.2-p.Thr140Met (n = 10, p = 0.39). Of these, only the conductance of p.Thr140Met alone differed from WT significantly.

To further study the voltage range around the resting membrane potential of skeletal muscle, extracellular KCl was decreased to 5 mM and the starting potential adjusted to – 140 mV. Plotting of these current peaks against the voltage revealed linear to saturated current-voltage relationships and reduced current densities compared to WT (Fig. 2D). Conductances for the inward current were 840.48 ± 98.62 nS/pF for WT (n = 10), 530.26 ± 82.47 nS/pF for p.Gly419Ser (n = 11, p = 0.19), 523.08 ± 62.29 nS/pF for p.Ile283Val (n = 11, p = 0.06), 614.29 ± 73.16 nS/pF for p.Cys75Tyr (n = 11, p = 0.18), and 1.51 ± 0.43 nS/pF for p.Thr140Met (n = 15, p < 0.001). This suggests that only p.Thr140Met reduced channel function.

Since the homologous Kir2.1 is the main skeletal muscle potassium channel maintaining the resting

membrane potential, along with Kir2.2 (13) we investigated the effects of the variants on heteromeric Kir2.2-Kir2.1 channels by co-transfecting the two plasmids at an equimolar ratio. As expected by the literature (14), WT Kir2.1/WT Kir2.2 co-expression showed a significantly higher current density at 5 mM extracellular KCl at -130 mV (– 737.06 ± 113.27 pA/pF, n = 14) compared with expression of WT Kir2.1 alone (– 491.82 ± 48.18 pA/pF, n = 17, p = 0.04) which indicates formation of functional hetero-tetramers in our experimental conditions (Fig. 3A). Plotting of the obtained current peaks against the voltage revealed linear to saturated current-voltage relationships (Fig. 3B). Conductances for the inward current were 1036.91 ± 151.97 nS/pF for WT (n = 14), 529.66 ± 75.37 nS/pF for p.Gly419Ser (n = 16, p = 0.01), 624.91 ± 110.25 nS/pF for p.Ile283Val (n = 17, p = 0.03), 552.36 ± 92.89 nS/pF for p.Cys75Tyr (n = 17, p = 0.01), and 134.11 ± 48.99 nS/pF for p.Thr140Met (n = 19, p < 0.001). This suggests that all variants reduced co-expressed Kir2.1 function to some degree with p.Thr140Met being the most potent which may elicit a so-called dominant-negative effect on Kir2.1 by reducing conductance by 87% in our experiment.

Molecular modelling

To confirm a dominant negative effect of Kir2.2 with p.Thr140Met on WT Kir2.1, we created three-dimensional models of Kir2.2-Kir2.1 hetero-tetramers (Fig. 4A, B). These were equilibrated for energy minimization using Chimera, and compared for the WT Kir2.2-Kir2.1 tetramer, p.Thr140Met Kir 2.2-WT Kir2.1 tetramer (2:2) and for p.Thr140Met Kir 2.2-WT Kir2.1 (3:1), p.Thr140Met Kir 2.2 chains. For the Kir WT 2.2-2.1 tetramer in equimolar model ratio, energy minimization resulted in a re-distribution of potassium ions towards the putative binding sites in the pore helix of Kir 2.2 compatible with a higher maximal current of the hetero-tetramer (Fig. 4C). For the Kir p.Thr140Met 2.2-Kir WT2.1 tetramer in equimolar model ratio, re-distribution of potassium ion was minimal (Fig. 4D), and this effect was even more pronounced when 3 Kir p.Thr140Met 2.2 chains were used in construction of the tetramer (Fig. 4E). These findings support the functional results showing that p.Thr140Met reduces the maximal current of the hetero-tetramer.

In order to quantify the effect of the variant, molecular dynamics simulations for the WT Kir2.2-Kir2.1 tetramer *versus* p.Thr140Met Kir 2.2-WT Kir2.1 tetramer (2:2) were performed. They revealed two significant differences between the WT Kir2.2-Kir2.1 model (Fig. 5A) and Thr140Met Kir 2.2-WT Kir2.1 model (Fig. 5B). The first was that the distance between center of mass at the distal carbon for adjacent residues in the pore helix of Glu139 and Thr140 (WT) or Met140 (variant) was significantly greater for the WT model (8.09 ± 0.43 Å) compared to the Thr140Met model (5.39 ± 0.52 Å, p ≤ 0.05, Fig. 5C). The second was that the H-bonding between Glu139 and Ile144 of the TIGYG selectivity filter was observed in 37.2% of frames for the WT model, but in no frames at all for the Thr140Met model (Fig. 5D). It is quite possible that the shorter distance between side chains of the Glu139 and Met140 compared to that for Glu139 and Thr140 may contribute to the loss of hydrogen bonding in the Thr140Met model.

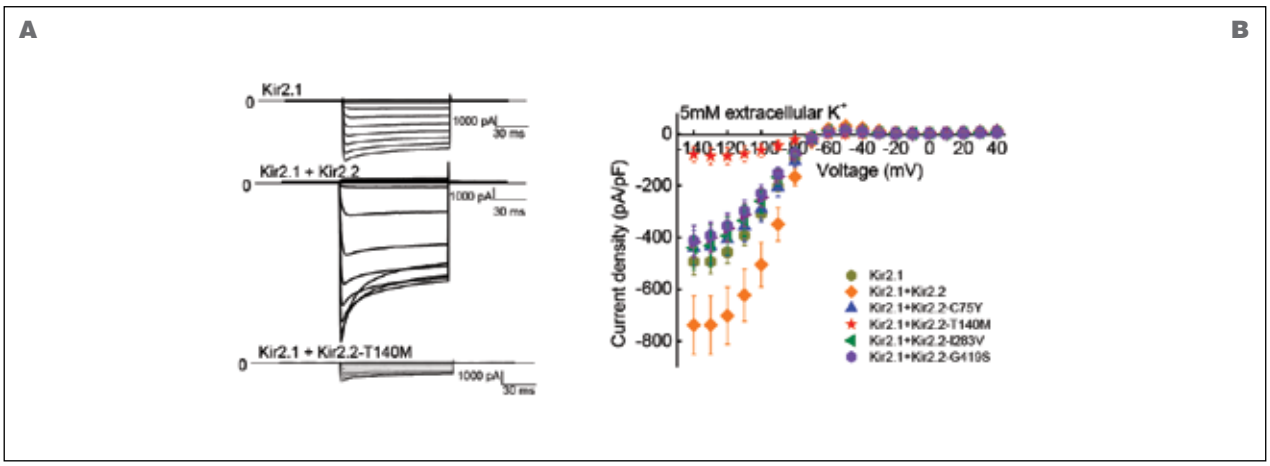

Figure 3. *Co-expression of Kir2.1.* Functional characterization of hetero-tetramers between Kir2.1 and Kir2.2-WT and four missense variants expressed in tsA 201 cells. **A)** Representative current traces. **B)** Normalized current-voltage relationships for WT Kir2.1 (n = 17), WT/WT Kir2.1 + Kir2.2 (n = 14), WT Kir2.1+Kir2.2-p.Cys75Tyr (n = 17), WT Kir2.1 + Kir2.2-p.Thr140Met (n = 19), WT Kir2.1 + Kir2.2-p.Ile283Val (n = 17) and WT Kir2.1 + Kir2.2- p.Gly419Ser (n = 16) recorded in 5mM external K+. Data are shown as means ± SEM.

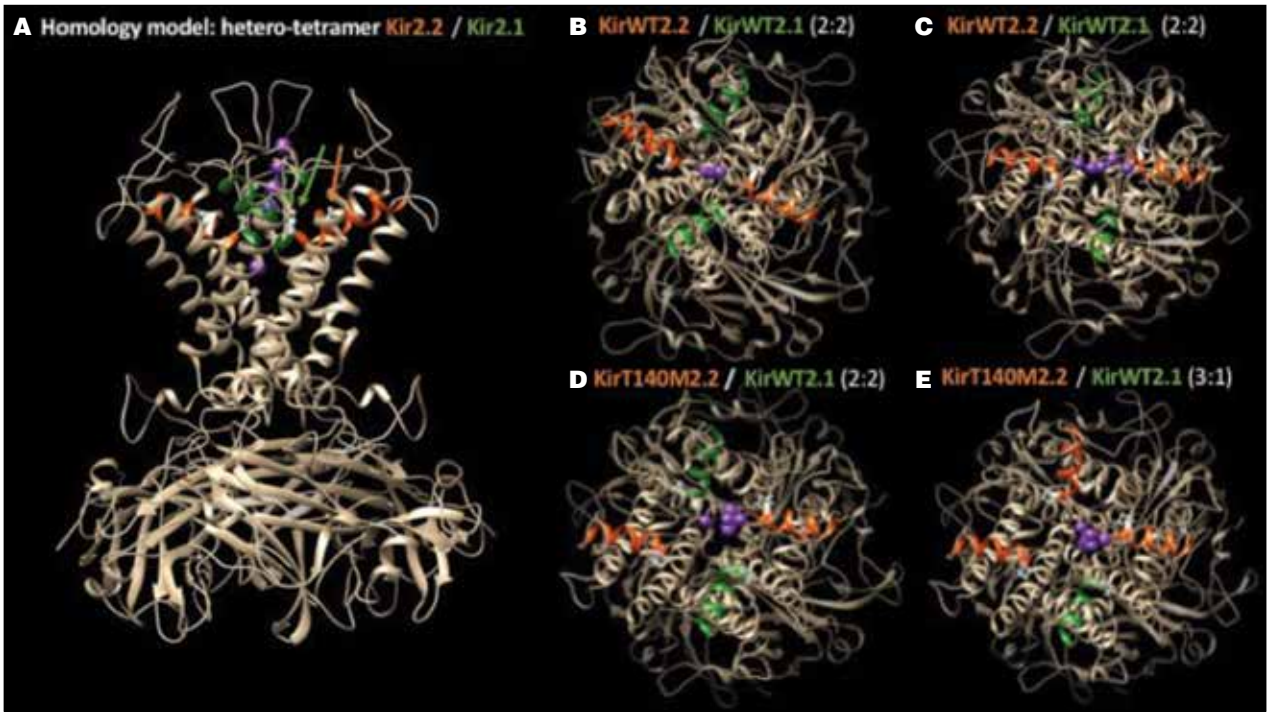

Figure 4. *Homology models.* Homology models of Kir2.2 and Kir2.1 incorporated into a tetramer of equimolar ratio **A)**. Pore helical regions are colored orange (Kir2.2) or green (Kir2.1), with homologous pore helix residues Thr140 (Kir2.2) and Thr139 (Kir2.1) shown in white with corresponding arrows; potassium ions are included with chain A (Kir2.2, right) from the original 4lp8 pdb coordinates. Top view of same prior to equilibration is shown in **B)**. After equilibration for energy minimization, top views show relative re-distribution of potassium ions for the WT equimolar heterotetramer **C)**, and with variant p.Thr140Met incorporated into 2 Kir2.2 chains **D)** or 3 Kir2.2 chains **E)**. The Kir2.2 p.Thr140Met variant resulted in less movement of the potassium ions towards binding sites in the pore helix.

Discussion

Based on the Sanger sequencing data, it is clear that non-synonymous Kir2.2 variants are infrequent; we found 4 in 264 patient samples (1.5%) a frequency similar to a previous study of the homologous channel Kir2.6 which detected 10 variants in 263 patient samples (3.8%) (8). Three of the variants, p.Gly419Ser, p.Ile283Val, and p.Cys75Tyr, are all located in cytoplasmic regions of the Kir2.2 channel. p.Gly419Ser is a known benign polymorphism named rs77266866 (dbSNP database, www.ncbi.nlm.nih.gov/snp/) which slightly depressed co-expressed Kir2.1. The two novel variants, p.Ile283Val, and p.Cys75Tyr, presented with functional effects of a similar degree. Therefore, all three variants may be interpreted as benign functional polymorphisms according to Jurkat-Rott and Lehmann-Horn 2005 (15). In contrast, p.Thr140Met is located in a transmembrane pore-forming alpha helix close to the selectivity filter (amino acid residues 143-148). It produced a loss of Kir2.2 function and supressed co-expressed WT Kir2.1. This may indicate a susceptibility or potentially pathogenic variant.

The prediction programs were not reliable in determining the functional effects since of the two variants which both were consistently predicted to be pathogenic, p.Cys75Tyr and p.Thr140Met, only one had significant functional effects. In contrast, three variants had comparable function but very different prediction results: p.Gly419Ser which was consistently predicted to be benign and the two novel variants, p.Ile283Val and p.Cys75Tyr, one of which was consistently predicted to be pathogenic. This assessment is in agreement with previous studies on the quality of prediction programs in ion channelopathies which found reasonable sensitivities ranging from ~ 70-90% but low specificities of ~ 15-50% depending on channel type and protein regions within the channels (16, 17).

Our data show that the loss of function of p.Thr140Met Kir2.2 is not due to a trafficking defect but results from an alteration of the ion pore conductance. Together with the dominant negative effect on the main skeletal muscle rectifying potassium channel, Kir2.1, the functional effects are very similar to those of the PP Mutations in Kir2.6 which also display a loss of function and suppress co-

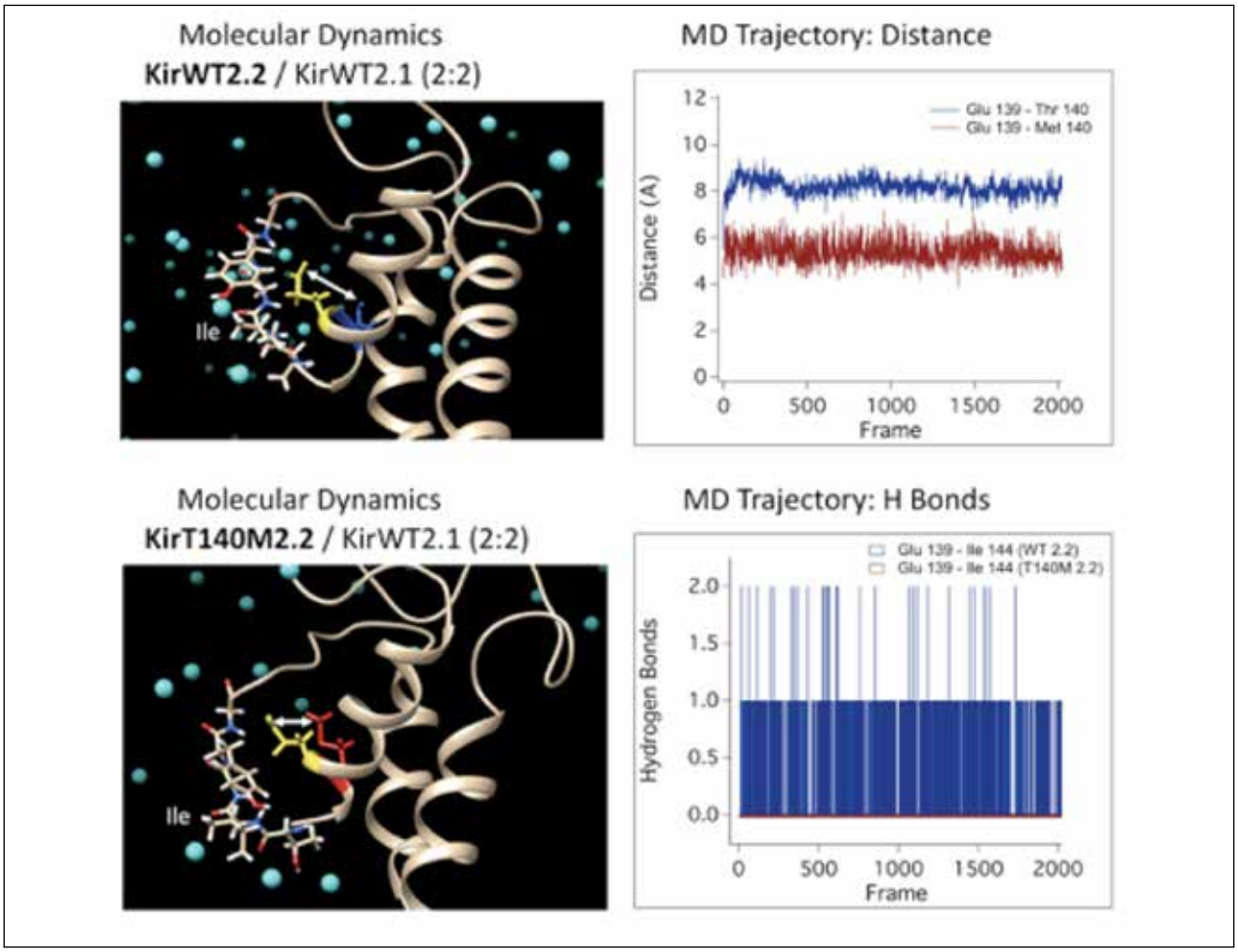

Figure 5. *Molecular dynamics simulations.* Models of equimolar Kir2.2 and Kir2.1 were incorporated into a POPC membrane, solvated and ionized, and subjected to an electric field for molecular dynamics simulations. The pore helix of one Kir2.2 chain and the TIGYG selectivity filter are shown in panels **A)** (WT 2.2) and **B)** (Thr140M 2.2), along with potassium ions (cyan). Distance measurements between the pore helix Glu139 (yellow) and Thr140 (blue, panel **A**) or Met140 (red, panel **B**) are depicted by the white arrows, and are calculated from MD trajectories shown in panel **C)**. Hydrogen bonding between Glu139 and the Ile144 of the selectivity filter are calculated from trajectories shown in panel **D)**. Reduced distance between pore helix residues Glu139/Met140 in the variant compared to Glu139/Thr140 in WT is correlated with an absence of hydrogen bonding between Glu139 and the target Ile144 of the selectivity filter.

expressed Kir2.1. (12, 18). Additionally, the same amino acid change, i.e. p.Thr140Met, in the highly homologous Kir2.6 channel has been shown to cause a similar phenotype, TPP (12), which supports the notion of susceptibility or potential pathogenicity of p.Thr140Met in Kir2.2.

As to the dominant negative effect on Kir2.1, loss of function mutations in the encoding *KCNJ2* gene are known to cause Andersen-Tawil Syndrome, a PP phenotype with the additional features cardiac arrhythmia and facial dysmorphia (5). However, our patient did not have such symptoms nor did the TPP patients with Kir2.6 mutations described previously (12). To clarify this conundrum, we compared public data of quantitative tissue-specific expression patterns. According to the Genotype Tissue Expression Consortium (www.gtexportal.org), the following RNA expression levels in reads per kilobase per million mapped reads have been found for *KCNJ12 vs KCNJ2*: for skeletal muscle 12.3 *vs* 1.0, for heart 2.9 *vs* 2.3, and for skin 3.6 *vs* 0.9. Data from another source, the Human Protein Atlas (www.proteinatlas.org), lists the following transcripts per million: for skeletal muscle 23.1 *vs* 3.3., for heart 3.9 *vs* 6.3, and for skin 2.1 *vs* 5.6. The Fantom5 Consortium (www.fantom.gsc.riken.jp) has published the following expression levels in tags per million: for skeletal muscle 19.1 *vs* 8.1, for heart 7.4 *vs* 23.9, and for skin no data is available. All three sources agree that *KCNJ12* ex-

pression in skeletal muscle is at least two times larger than *KCNJ2*. This is not the case for heart and skin.

Possible phenotypes may be suggested by knockouts. While KCNJ2 knockout mice die within hours after birth due to severe dysmorphia (cleft palate) and show no Kir currents in arterial myocytes, *KCNJ12* knockouts are viable and fertile and without dysmorphia (19). Suppression of Kir2.1 in heart leads to reduction of the cardiac Kir current by 95% (20). Taken together, expression levels and knockout data suggest that Kir2.2 mutations are most likely, if not exclusively, to cause muscle symptoms and not dysmorphia or cardiac arrhythmia.

Assuming a relative abundance of *KCNJ12* to *KCNJ2* of 2:1, there would be an equimolar ratio of WT Kir2.2 to p.Thr140Met Kir 2:2 to WT Kir2.1, i.e. of 1:1:1. Heterotetramers with none, one, or several p.Thr140Met may be present. Our molecular modelling demonstrated that the incorporation of an increasing number of Kir2.2 p.Thr140 in heterotetramers with Kir2.1 decreased the movement of potassium ions towards their binding sites in the pore helix which directly results in current reduction. Quantification by molecular dynamics simulations demonstrated that the incorporation of Kir2.2 p.Thr140 in heterotetramers with Kir2.1 resulted in loss of formation of hydrogen bonding between Glu139 and Ile144 of the selectivity filter. This interaction is important in early permeation steps in KcsA channels (11), supporting the hypothesis that current reduction in heterotetramers containing the p.Thr140Met Kir 2:2 variant may be, at least partly, the consequence of the observed reduction in hydrogen bonding. Whether or not the current reduction is enough to reduce the total inward Kir current sufficiently to cause PP determines the difference between pathogenic variant and susceptibility (15).

Additionally, there may be genetic background factors to take into account. In the proband with p.Thr140Met in Kir2.2, there were two additional, unknown, non-synonymous, possibly pathogenic, heterozygous variants: one in *PRKCQ* encoding protein kinase C theta (PKCθ) and one in *TTN* encoding titin. Both have previously not been linked to PP, but may still contribute to the phenotype of the proband. Titin mutations are known to cause multiple other diseases of heart and skeletal muscle; namely several cardiomyopathies, limb-girdle dystrophy type 2, proximal myopathy with respiratory involvement, Salih myopathy, and tardive tibial muscular dystrophy (21, 22) and, therefore, titin variants could contribute to the manifestation of muscle weakness. For PKCθ, even though it has not been associated to disease at all, it is quite important for regulation of skeletal muscle function. PKCθ phosphorylates and thereby reduces the current amplitude of the muscular chloride channel ClC-1 (23) which helps muscle to uphold muscle excitability during exercise (24). An increased PKCθ could mimic the pathogenetic mechanism underlying the skeletal muscle disorder of myotonia congenita which is caused by muscle hyperexcitability due to decreased ClC-1 current (25). Alternatively, an inhibition of Protein kinase C – which may be expected to a. o. increase ClC-1 current – improves muscle regeneration in a mouse model of Duchenne muscular dystrophy (26) and could lessen the severity of a PP phenotype.

Taken together, the sporadic occurrence of SPP suggests that the pathogenic potency of Kir2.2 variants may be dependent on additional factors such as individual genetic background (i.e. co-existing variants in *PRKCQ* and *TTN*) or epigenetic phenomena. Therefore, we conclude that Kir2.2 p.Thr140Met may be most safely interpreted as a SPP susceptibility variant and it should be included in the genetic testing scheme for diagnosing SPP.

Acknowledgements

This study was supported by the non-profit Hertie Foundation, the German Federal Ministry of Research (BMBF IonNeurONet), the DGM German Muscle Disease Society, Taro Pharma, and NIH R15 NS09357901-A1. We thank Landon Bayless-Edwards (ISU) for invaluable assistance with computations from MD simulations.

References

1. Matthews E, Silwal A, Sud R, et al. Skeletal muscle channelopathies: rare disorders with common pediatric symptoms. J Pediatr 2017;188:181-5.
2. Cannon SC. Channelopathies of skeletal muscle excitability. Compr Physiol 2015;5:761-90.
3. Jurkat-Rott K, Groome JR, Lehmann-Horn F. Pathophysiological role of omega pore current in channelopathies. Front Neuropharmacol 2012;3:1-15.
4. Spillane J, Kullmann DM, Hanna MG. Genetic neurological channelopathies: molecular genetics and clinical phenotypes. J Neurol Neurosurg Psychiatry 2016;87:37-48.
5. Statland JM, Tawil R, Venance SL. Andersen-Tawil syndrome. In: Adam MP, Ardinger HH, Pagon RA, et al., Eds. GeneReviews®. Seattle (WA): University of Washington, 1993-2018.
6. Li H, Durbin R. Fast and accurate short read alignment with Burrows-Wheeler transform. Bioinformatics 2009;25:1754-60.
7. Li H, Handsaker B, Wysoker A, et al. 1000 genome project data processing subgroup. The sequence alignment/map format and SAMtools. Bioinformatics 2009;25:2078-9.
8. Kuhn M, Jurkat-Rott K, Lehmann-Horn F. Rare KCNJ18 variants do not explain hypokalaemic periodic paralysis in 263 unrelated patients. J Neurol Neurosurg Psychiatry 2016;87:49-52.

9. Zubcevic L, Bavro VN, Muniz JRC, et al. Control of KirBac3.1 potassium channel gating at the interface between cytoplasmic domains. J Biol Chem 2014;289:143-51.
10. Pettersen EF, Goddard TD, Huang CC, et al. UCSF Chimera – a visualization system for exploratory research and analysis. J Comput Chem 2004;25:1605-12.
11. Berneche S, Roux B. A gate in the selectivity filter of potassium channels. Structure 2005;13:591-600.
12. Ryan DP, da Silva MR, Soong TW, et al. Mutations in potassium channel Kir2.6 cause susceptibility to thyrotoxic hypokalemic periodic paralysis. Cell 2010;140:88-98.
13. DiFranco M, Yu C, Quiñonez M, et al. Inward rectifier potassium currents in mammalian skeletal muscle fibres. J Physiol 2015;593:1213-38.
14. Panama BK, McLerie M, Lopatin AN. Fuctional cosequences of Kir2.1/Kir2.2 subunit heteromerization. Pflugers Arch 2010;460:839-49.
15. Jurkat-Rott K, Lehmann-Horn F. Muscle channelopathies and critical points in functional and genetic studies. J Clin Invest 2005;115:2000-9.
16. Leong IU, Stuckey A, Lai D, et al. Assessment of the predictive accuracy of five in silico prediction tools, alone or in combination, and two metaservers to classify long QT syndrome gene mutations. BMC Med Genet 2015;16:34.
17. Flanagan SE, Patch AM, Ellard S. Using SIFT and PolyPhen to predict loss-of-function and gain-of-function mutations. Genet Test Mol Biomarkers 2010;14:533-7.
18. Cheng CJ, Lin SH, Lo YF, et al. Identification and functional characterization of Kir2.6 mutations associated with non-familial hypokalemic periodic paralysis. J Biol Chem 2011;286:27425-35.
19. Zaritsky JJ, Eckman DM, Wellman GC, et al. Targeted disruption of Kir2.1 and Kir2.2 genes reveals the essential role of the inwardly rectifying K(+) current in K(+)-mediated vasodilation. Circ Res 2000;87:160-6.
20. McLerie M, Lopatin AN. Dominant-negative suppression of I(K1) in the mouse heart leads to altered cardiac excitability. J Mol Cell Cardiol 2003;35:367-78.
21. Chauveau C, Rowell J, Ferreiro A. A rising titan: TTN review and mutation update. Hum Mutat 2014;35:1046-59.
22. Savarese M, Sarparanta J, Vihola A, et al. Increasing role of Titin mutations in neuromuscular disorders. J Neuromuscul Dis 2016;3:293-308.
23. Camerino GM, Bouchè M, De Bellis M, et al. Protein kinase C theta (PKCθ) modulates the ClC-1 chloride channel activity and skeletal muscle phenotype: a biophysical and gene expression study in mouse models lacking the PKCθ. Pflugers Arch 2014;466:2215-28.
24. Riisager A, de Paoli FV, Yu WP, et al. Protein kinase C-dependent regulation of ClC-1 channels in active human muscle and its effect on fast and slow gating. J Physiol 2016;594:3391-406.
25. Imbrici P, Altamura C, Pessia M, et al. ClC-1 chloride channels: state-of-the-art research and future challenges. Front Cell Neurosci 2015;9:156.
26. Marrocco V, Fiore P, Benedetti A, et al. Pharmacological Inhibition of PKCθ counteracts muscle disease in a mouse model of Duchenne muscular dystrophy. EBioMedicine 2017;16:150-61.